Research Article

Facile synthesis of nanocrystalline β-$SnWO_4$: as a photocatalyst, biosensor and anode for Li-ion battery

N. S. Pavithra[1] · Shivaraj B. Patil[1] · S. R. Kiran Kumar[2] · Fahad A. Alharthi[3] · G. Nagaraju[1]

Abstract

Here, we have successfully synthesised β-$SnWO_4$ Nps via simple and low-cost co-precipitation method. XRD pattern confirms the wolframite cubic structure of β-$SnWO_4$ Nps which is belonging to P_{213} or T^4 space group with an average crystallite size of ~38 nm. FTIR spectrum of β-$SnWO_4$ Nps shows the bands at 620–825 cm^{-1} is assigned to characteristical stretching and bending vibrational modes of WO_6^6, W–W bonds and stretching vibration of W–O–W bridging bonds in β-$SnWO_4$. UV-DRS spectrum shows the strong absorption band edge at 604 nm and the estimated bandgap of β-$SnWO_4$ Nps is found to be 1.9 eV. The β-$SnWO_4$ shows excellent photocatalytic activity against indigo carminedye under various conditions of β-$SnWO_4$ Nps. In addition to this, the electrochemical senor performance toward the quantification of dopamine at nanomolar concentration and anode material for Li-ion batteries by showing high reversible discharge/charge capacity was explored.

Keywords β-$SnWO_4$ · Photocatalytic degradation · Biosensing · Li-ion battery

1 Introduction

Nanostructured materials find several applications in various nanodevices such as field-effect transistors, biochemical sensors, nanocables, energy storage devices, etc. In particular, energy storage and catalysis-related research is one of the major challenges in the present scenario. Energy crisis and environmental deterioration makes the semiconductor photocatalysts attracted worldwide due to their potential applications in energy conversion and degradation of organic pollutants in wastewater [1]. In recent decades, the development of the agrochemical industry has increased dramatically due to widespread intensive pharmaceutical and agricultural activities. Many industries produce huge amount of chlorinated compounds which is contaminating the freshwater (surface and groundwater), coastal and marine environments which leads to the serious environmental problems. Heterogeneous semiconductor photocatalysis has become an attractive method for remediating environmental contamination due to its high photocatalytic activity, non-toxicity and photostability. Photocatalytic water purification technology is considered as one of the promising application as it remove/separate the organic pollutants produced by the agricultural, textile and pharmaceutical industries. From the last few years, more research has been devoted to minimalizing such environmental problems [2–6]. Photocatalysis refers to the acceleration of chemical reactions (oxidation/reduction) at the catalyst surface under ultraviolet (UV) or visible radiation. Photocatalysis occurs when catalyst was exposed to UV light resulting in the formation of holes in the valence bond (VB) [7] and electrons are excited to the conduction band (CB). Meanwhile, hydroxyl radicals are formed which are necessary for the complete mineralization of dye molecules into CO_2 and H_2O [8]. Various processes have been performed such as

✉ G. Nagaraju, nagarajugn@rediffmail.com | [1]Department of Chemistry, Siddaganga Institute of Technology (Affiliated to Visvesvaraya Technological University-Belagavi), Tumakuru, Karnataka 572 103, India. [2]Department of Chemistry, K S Institute of Technology, Bengaluru 560 109, India. [3]Department of Chemistry, College of Science, King Saud University, P.O. 2455, Riyadh 11451, Saudi Arabia.

SN Applied Sciences (2019) 1:1123 | https://doi.org/10.1007/s42452-019-1163-3

Received: 10 January 2019 / Accepted: 23 August 2019 / Published online: 30 August 2019

adsorption, reverse osmosis and activated carbon have been performed to remove the dye molecules in the water reservoirs released from industries [9].

Electrochemical sensors provide an attractive ways to analyze the content of a target sample due to the direct conversion to an electronic signal. Electrochemical biosensors are at the forefront of a multidisciplinary science that combines electrochemistry and biology [10]. Sensing of bio-molecules such as dopamine (DA) or catecholamine attracts the researchers because of its vital role in analyzing and estimating organ systems such as central nervous system, hormonal, cardiovascular and renal stems. DA deficiency causes many serious diseases and sickness such as Parkinson's disease, HIV infection and schizophrenia etc. [11] DA is not only a significant catecholamine neurotransmitter in the human brain, but also used as an intravenous medicine used to raise heart rate and blood pressure. Thus, in common medical exercise, trace level determination of DA in vivo/vitro is vital for finding pathological conditions and also for developing forthcoming diagnostic approaches compared with other techniques [12].

In the past 20 years, extensive efforts have been made to improve the electrochemical behaviour of the group IV elements (Si, Ge, Sn) based anode [13]. It is critical that low-cost, light-weight, small-volume and echo-friendly energy storage/conversion devices must be developed. Nowadays nanomaterials are of great interest to be used as electrode materials for rechargeable lithium ion batteries (LIBs) [14]. LIBs play an important role in the current profile due to their high gravimetric and volumetric energy, high cycle life, high power density and long self-discharge properties [15]. The most effective approaches include: (1) reducing particle size to nanoscale for alleviating mechanical strain: (2) forming the hierarchical porous structure to provide a stable solid electrophilic interphase layer of the inner pore that provides adequate space for expansion; dispersing amorphous nano-sized materials [16]. Lithiation/delithiation of Li^+ ions during charge/discharge correlates with a change in the oxidation state of transition metal electrodes [17]. According to the literature survey, $SnWO_4$ Nps have been considered as an excellent photocatalyst for catalytic dye degradation and also it shows good electrochemical performances. Many researchers have carried out photocatalytic activity using β-$SnWO_4$ Nps. For example, Ying et al., synthesized β-$SnWO_4$ observed textural alteration leads to enhanced the photocatalytic activity for dye degradation [18]. Jan Ungelenka and Claus Feldmann have synthesized bulk β-$SnWO_4$ and nano β-$SnWO_4$ materials to study the photocatalytic activity of methylene blue [19]. H T Chandran et al., synthesized β-$SnWO_4$ Nps for visible light driven sonocatalytic degradation of Resazurin dye and observed enhanced results [20]. Raj et al. synthesized β-$SnWO_4$ Nps via sonication method and reported good photocatalytic dye degradation against methyl orange dye [21]. In addition to examine photocatalytic application, we have also performed the electrochemical dopamine sensing and as a electrode materials for lithium ion battery (LIB) applications. Few reports are available on $SnWO_4$ NPs, which acts as a good anode material for LIB [22, 23] .

We have synthesized surfactant assisted β-$SnWO_4$ Nps using simple co-precipitation techniques. This method does not require any high temperature/pressure withstanding equipments. We have prepared β-$SnWO_4$ Nps using stannous chloride with sodium tungstate precursors in the presence of cetrimide as surfactant in acidic (citric acid) medium. Here, surfactant plays a very important role for the synthesis of nanomaterials. In an aqueous solution, the surface adsorption of surfactant molecules takes place through bilayer formation, which prevents the agglomeration [24] and thus reduces the crystal size. Citric acid is a buffer solution that maintaining the pH of the solution and also excellent chelating agent to form complexes with the metallic cations, binding metals by making them soluble. But, till to date no work has been done by taking IC dye to measure the photocatalytic activity of these synthesized Nps. Therefore, we choose IC dye as the model pollutant system for the photocatalytic experiment. Electrochemical dopamine detection is attractive because it is simple, easy handle and more sensitive to detection. For this reason, we used β-$SnWO_4$ electrode to detect dopamine at nanomolar concentration. It was found that $SnWO_4$ is electrochemically active for sensors studies [25]. The selection of a good anode material that can provide high capacity and easy diffusion of Li-ion along with good cycling life and free from safety concern [26] research is still in progress. Thus, we have used pure β-$SnWO_4$ nanomaterial, as a promising anode material for Li-ion battery applications.

2 Experimental

2.1 Experimental synthesis

All the chemicals were purchased from analytical grade reagent without any further purification. Stannous chloride ($SnCl_2{\cdot}2H_2O$), Sodium tungstate ($Na_2WO_4{\cdot}2H_2O$) were purchased from Merck India Ltd. Cetrimide and Citric acid used were received from SD Fine Chemicals limited and de-ionized water was used for the entire synthesis and application purposes. In typical synthesis, Solution A was prepared using 1.128 g of $SnCl_2{\cdot}2H_2O$ dissolved in 10 ml of ethanol. Solution B was prepared by dissolving 100 mg of cetrimide (cetyl trimethyl ammonium bromide) in 50 ml of de-ionised water; followed by adding 10 ml of 0.1 M citric acid to achieve acidic medium. To the above acidic solution (B), solution A was mixed and stirred at 940 rpm to

obtain a homogeneous solution. 1.649 g of $Na_2WO_4{\cdot}2H_2O$ crystals were added, immediately yellow precipitate of $SnWO_4$ is formed. The obtained product was collected, centrifuged and washed with distilled water /ethanol. The yellowish mass was subjected to calcination at 400 °C, 600 °C and 800 °C for 2 h. Figure 1 shows the schematic representation of the different steps involved in the synthesis of β-$SnWO_4$ nanomaterial. Finally, the calcined product (800 °C/2 h calcined) was used for structural characterization and for various applications, including photocatalytic activity, electrochemical sensing and Li-ion battery.

2.2 Structural, optical and morphological characterization

X-Ray diffraction (XRD) data of β-$SnWO_4$ nanoparticles were collected with Rigaku smart lab X-ray diffractometer using graphite monochromatized Cu Kα radiation (l = 1.541 A). FTIR analysis was used to determine the functional groups (Bruker Alpha-P spectrophotometer) where the spectra were recorded from 400 to 4000 cm^{-1}. UV-Visible diffused reflectance spectra were analysed by Perkin Elmer Lambda-35 spectrophotometer at room temperature. Morphologies of the products were examined using JSM-6490LB scanning electron microscope and JEOL 3010 Transmission electron microscope (TEM) equipped with a Gatan CCD camera operating at an accelerating voltage of 300 kV.

2.3 Photocatalytic reactions

Photocatalytic activity of β-$SnWO_4$ (800 °C) nanoparticles were carried out by the degradation of IC dye in a photocatalytic reactor (Heber photoreactor, model:HVAR 123, annual-visible type). Here, we have selected IC as a model pollutant for photocatalytic experiments. Known quantity of photocatalyst was added to an appropriate volume of dye solution (100 ml). The suspension was kept in a dark for 30 min with aeration to ensure adsorption/desorption equilibrium between the IC and photocatalyst, then exposed to 300 W mercury lamp light. During visible light irradiation, 2 mL of the suspension was collected from the reaction solution at an interval of 30 min each and centrifugation was carried out for catalyst separation using spinwin microcentrifuge. Then, the supernatant solution was monitored using UV-Visible spectrophotometer (Agilent Carry 60) at λ_{max} 610 nm (IC) wavelength. Percentage of dye degradation was calculated as follows.

$$\text{Percentage of degradation} = \frac{C_i - C_f}{C_i} \times 100 \quad (1)$$

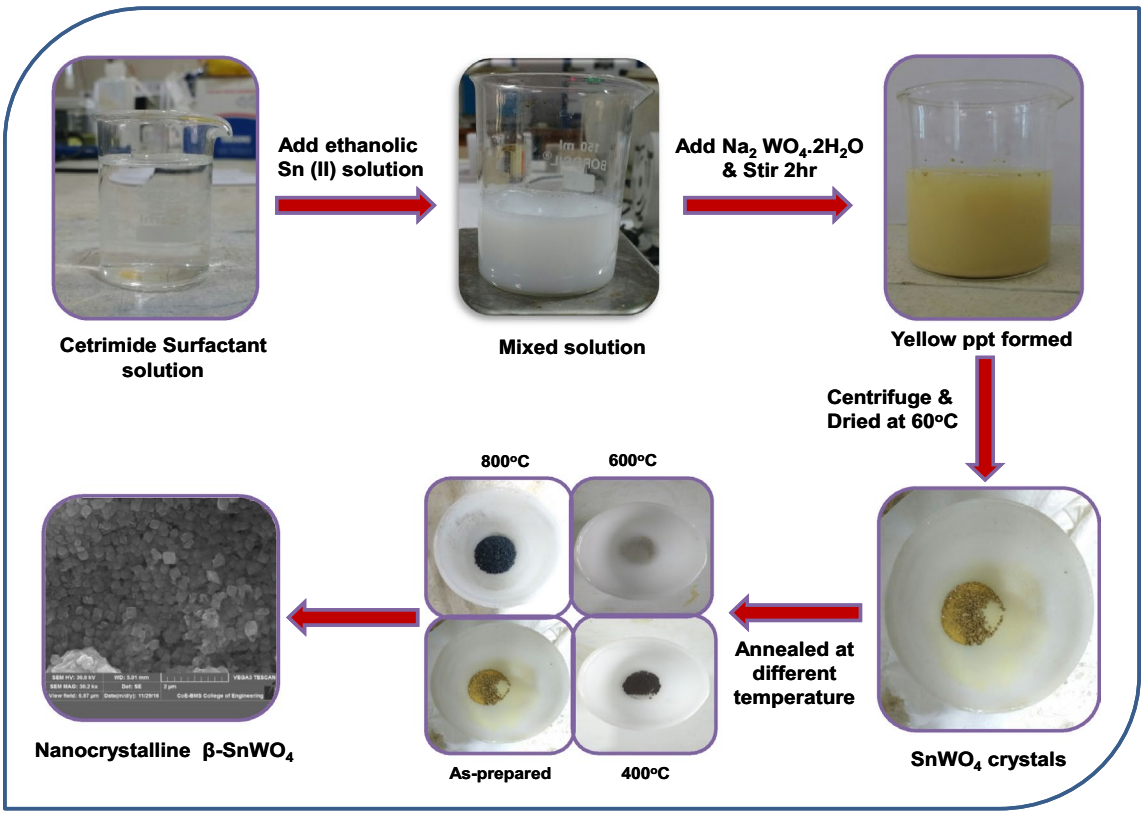

Fig. 1 Schematic representation for the steps involved in the synthesis of β-$SnWO_4$Nps

where C_i and C_f are the initial and final concentration of dye solution in ppm, respectively. The experimental procedure was repeated by changing various parameters such as dye variation, catalyst load, pH of the dye solution and catalyst recycling.

2.4 Electrocatalytic determination of dopamine as analyte using modified carbon paste electrode (MCPE)

The surface of the glassy carbon electrode was washed thoroughly with de-ionized water and sonicate for 5 min to remove the adhered particle on the surface of the electrode. The bare carbon paste electrode was prepared using graphite powder (80%) and silicon (20%) oil in a mortar and then air dried for overnight. This paste was packed into the cavity of the electrode and then smoothened on weighing paper. Similarly, adding an aqueous colloidal solution of β-$SnWO_4$ (800 °C) Nps (2, 4, 6 and 8 mg of Nps) to the above-mentioned mixture to make it modified carbon paste electrode. Cyclic voltammetry (CV) studies were carried out using CHI 660D Austin USA, consisting Ag/AgCl as a reference electrode and platinum wire as contour electrode. CV was recorded for bare as well as β-$SnWO_4$ Nps modified glassy carbon electrode in the known concentration of dopamine as the catalyst using phosphate buffer solution of pH 7.2.

2.5 Electrode fabrication for Lithium ion battery

Electrochemical performance was studied by the fabrication of electrodes and were prepared by dispersing electroactive material i.e. β-$SnWO_4$ (75%), electroconductive carbon black (15%) and binder PVDF (polyvinylidene fluoride 10%) using N-methyl-2-pyrrolidine (NMP) as a solvent to form a homogeneous slurry. The obtained slurry was coated on copper foil and electrodes were dried at 100 °C in a vacuum oven for overnight. The half-cell electrodes were assembled in the inert Ar-filled glove box with Li metal as the counter/reference electrode. β-$SnWO_4$(800 °C) Nps were used as the working electrode. 1 M $LiPF_6$ dissolved in ethylene carbonate and diethylene carbonate (1:1 volume %) as electrolyte. The galvanostatic charge–discharge tests were performed between 0.01 and 3 V vs. Li/Li^+. Cyclic voltammogram studies and the charge-discharge performances were recorded using Biologic BCS- 805 battery cycling system.

3 Results and disscusion

Figure 2a shows the X-ray diffraction pattern of the as-prepared and calcined β-$SnWO_4$ Nps at different temperature. As-prepared product shows the broad peak from 20° to 40° indicating the amorphous nature. As the calcined temperature increases to 600° crystallinity also increases. As the calcinations temperature reaches 800 °C, highly crystalline

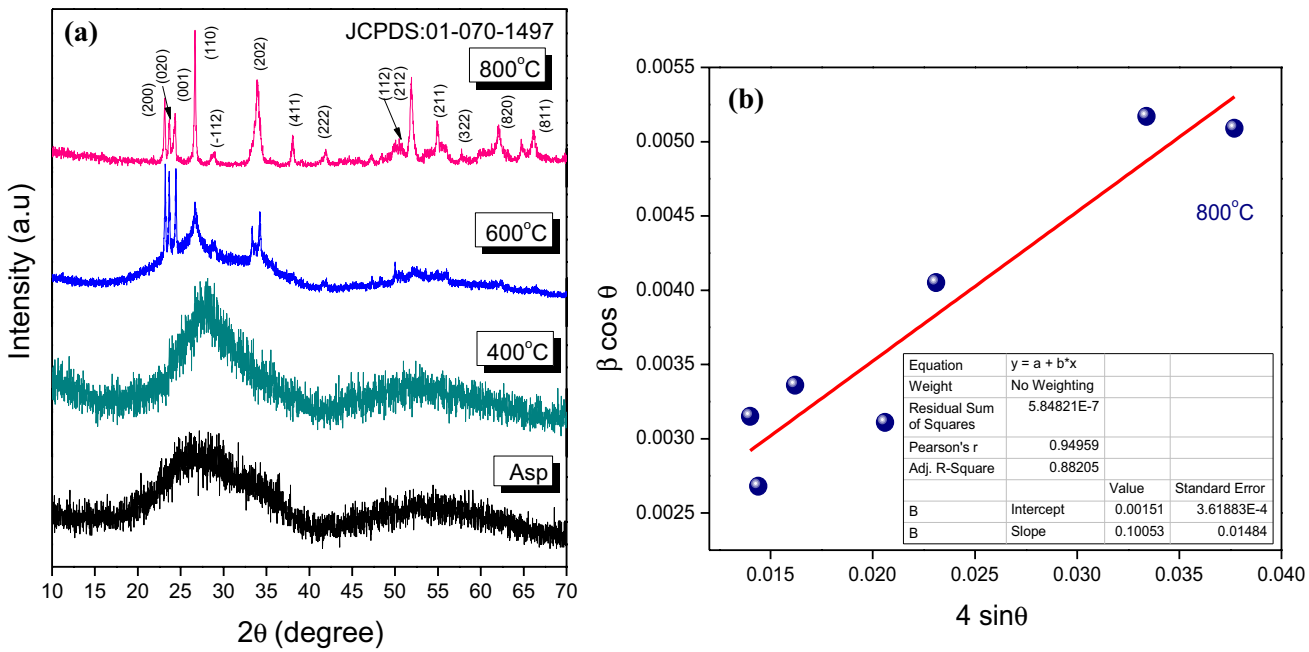

Fig. 2 **a** Powder X-ray diffraction pattern of β-$SnWO_4$ Nps calcined at different temperature. **b** W–H plots for β-$SnWO_4$ nanoparticle calcined 800°C

β-$SnWO_4$ Nps was obtained. All the diffraction peaks were indexed to wolframite cubic structure of β-$SnWO_4$Nps and matches well with the JCPDS Card No. 01-070-1497 [20, 21]. Sivasankara Rao Ede and Subrata Kundu observed similar type of XRD pattern for β-SnWO4 nanomaterials. So from the XRD analysis we confirmed that the synthesized SnWO4 NPs are pure and crystalline in nature [16]. The cubic structure of β-$SnWO_4$ belonging to ($P2_13$ or T^4) space group [27]. It is built up of slightly deformed WO_4 tetrahedra, which are interconnected with strongly distorted via SOJT effect [28]. WO_4 tetrahedra are slightly distorted with three short (1.747 Å) and one long (1.764 Å) W–O bonds. The W–O bond lengths depend on number of tin atoms are bound to the oxygen atom: the distant oxygen atom is shared with three tin atoms, whereas nearest three oxygen are bridging to one tin atom each [29]. The crystallite size was calculated using Scherer's formula (formula 2) and was found to be around 38 nm.

$$D = \frac{0.9\lambda}{\beta \cos\theta} \tag{2}$$

where D is crystallite size, β is the full-width at half maximum, λ is the wavelength of the radiation and θ is the angle of diffraction. According to the Williamson and Hall (W–H) plot particle size and strain of Nps have been determined using this equation.

$$\beta \cos\theta = \frac{K\lambda}{D} + 4\varepsilon \sin\theta \tag{3}$$

where ε represents micro strain and $\frac{K\lambda}{D}$ intercept. The graph (Fig. 2b) is plotted by taking β Cos θ (y-axis) and 4 Sin θ on (x-axis). The slope of the straight line gives the strain (ε), intercept (0.91/D) and y-axis give the crystallite size (D) respectively.

Figure 3 depicts the FTIR spectra of β-$SnWO_4$ Nps recorded from 400-4000 cm^{-1}. High intense broad peak at 3437 cm^{-1} and also strong peak at 1624 cm^{-1} observed for the hydroxyl (OH) stretching and bending vibrations. The peaks at 1221 cm^{-1} are structural vibrations of C–O–C or C–C bonds. The peaks observed at 621, 742 and 822 cm^{-1} correspond to asymmetric stretching vibration modes of WO_6^6, W–W bonds and stretching vibration of W–O–W bridging bonds in β-$SnWO_4$. All the above peaks observed confirmed the successful formation of β-$SnWO_4$ [30].

The diffused reflectance spectra of the samples were recorded from 200 to 1100 nm using barium sulphate as the reference material. Modified Tauc equation called Kubelka–Munk equation is used to determine the electronic band-gap of the solid samples [31]. Figure 4 shows the strong absorption band edge at 604 nm and the estimated band-gap of β-$SnWO_4$ Nps is found to be 1.9 eV. It reveals the potential photocatalytic application. The bandgap was obtained from the plots of hv $f(R)^2$ vs. hv

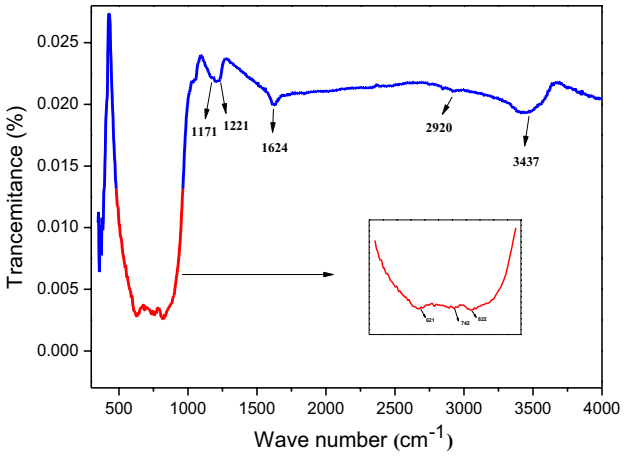

Fig. 3 FT-IR spectrum of β-$SnWO_4$ Nps

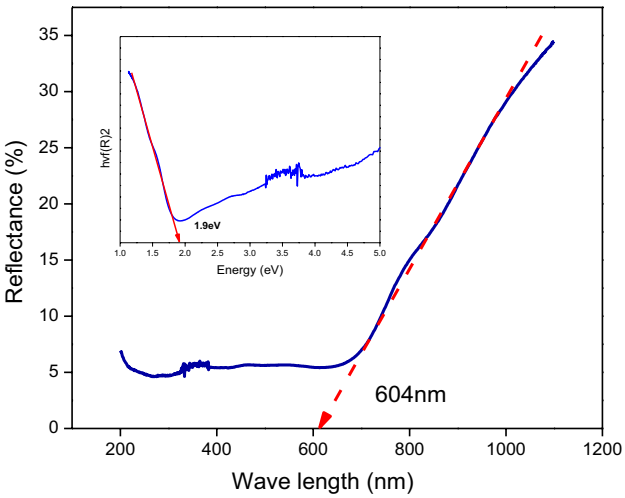

Fig. 4 DRS spectrum of β-$SnWO_4$nanoparticle (Kubelka-Munk plot) Inset: Tauc plat

(inset of Fig. 4a) by assuming the absorption coefficient is proportional to the Kubelka–Munk function hv $f(R)^2$ [32].

SEM images (Fig. 5) of as-prepared product shows agglomeration in nature. As the calcination temperature increases from 400 to 800 °C almost irregular shaped particles were observed. The TEM images (Fig. 6a and b) clearly show the particles nature. HRTEM images (Fig. 6c) shows the inter-planar lattice spacing of 0.260 nm corresponding to (202) facets of cubic β-$SnWO_4$ which supports the XRD results. Figure 6d image shows the selected area electron diffraction (SAED) pattern displays a bright spot pattern indicating the good crystallinity of the obtained product.

Figure 7 represents the schematic diagram of the photocatalytic degradation of IC dye as a targeted pollutant was used over photocatalyst. Photocatalytic experiment was carried out using 50 mg of catalyst in 2×10^{-5} M IC

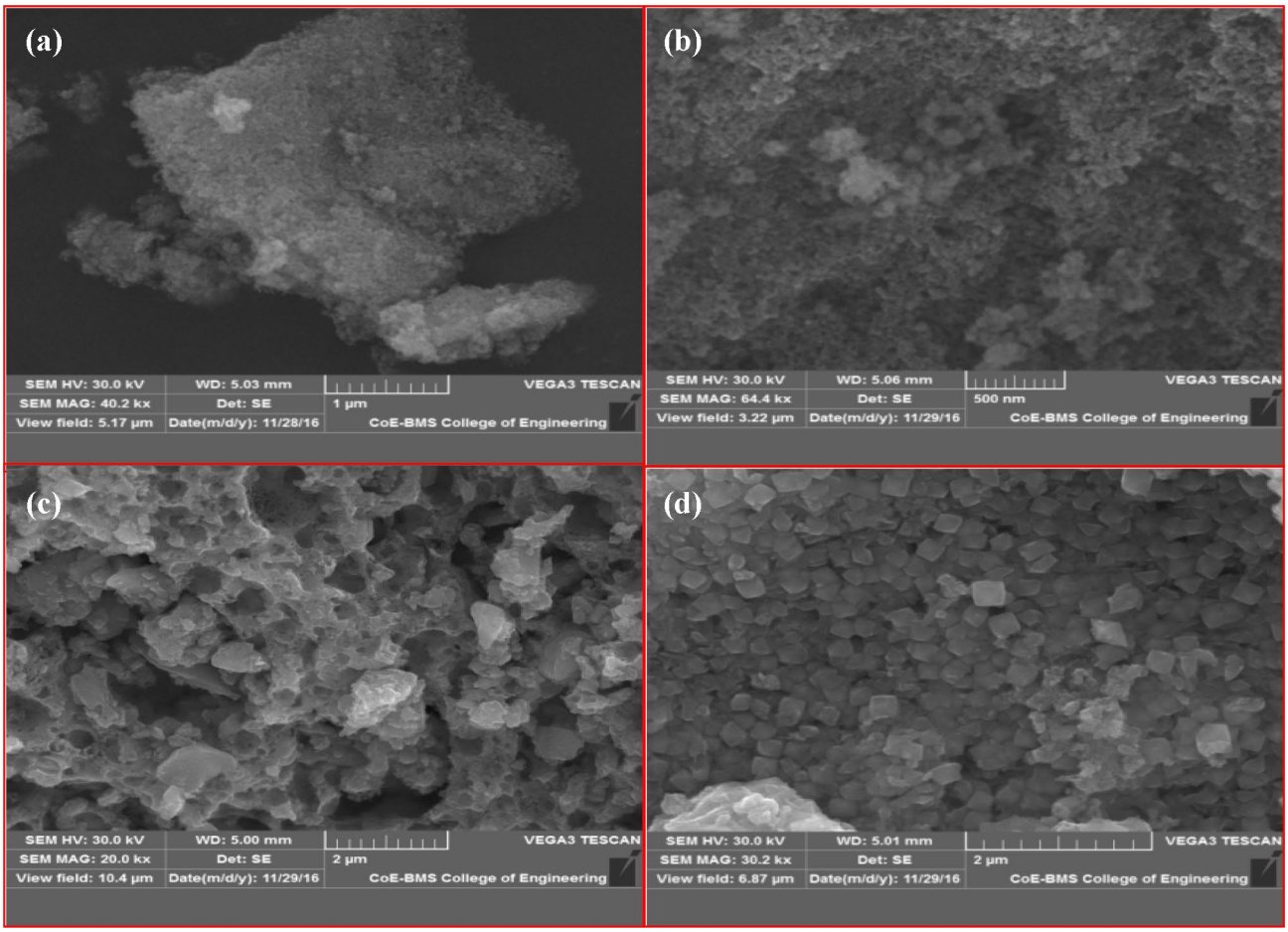

Fig. 5 SEM images of **a** as prepared, **b** 400 °C, **c** 600 °C and **d** 800 °C calcined β-$SnWO_4$ Nps

dye solution; this suspension was irradiated under visible light source. When a photocatalyst absorbs the photon of energy, which is higher than the bandgap of semiconductors, and then it creates electrons and holes in the valence band and conduction band. The β-$SnWO_4$ Nps shows lower bandgap (1.9 eV), smaller bandgap is normally effective for generating charge carriers and a higher surface area can additionally provide a larger number of active sites on the catalyst surface [33]. During degradation process, there is a production of highly reactive radicals (OH·, $O_2{\cdot}^-$, $HO_2{\cdot}$) takes place. These radicals are produced with the help of primary oxidants/energy sources (ex. Visible light) or catalysts (ex. β-$SnWO_4$). Chromophoric structure i.e. indigoid (NHC = CNH) group and secondary products are benzene *(Isatin sulfonic acid)* and carboxylic acid *(2-amine-5-sulfo-benzoic acid)* groups are observed in the region 210 to 260 nm of IC dye is destroyed via oxidation [34]. The decoloration of dye takes place after 120 min irradiation. The absorption maxima gradually decreased in terms of intensity at 610 nm wavelength, these observations are shown in Fig. 8a and probable reaction can be written as Eqs. (4–7) [21].

$$(\beta - SnWo_4) + hv(UV) \rightarrow (\beta - SnWo_4)(h^+_{VB}) + (\beta - SnWo_4)(e^-_{CB}) \quad (4)$$

$$(\beta - SnWo_4)(h^+_{VB}) + OH^- \rightarrow OH^\circ \quad (5)$$

$$(e^-_{CB}) + O_2 \rightarrow O_2^{-\circ} + (\beta - SnWo_4) \quad (6)$$

$$(\beta - SnWo_4) + OH^\circ + O_2^{-\circ} + Dye(IC) \rightarrow CO_2 + H_2O \quad (7)$$

Kinetic studies obtained by plotting $\ln(C_0/C)$ vs. irradiation time (min) was found to be straight line (Fig. 8b) which clearly indicates that degradation of dye over β-$SnWO_4$ Nps follows pseudo first order reaction kinetics in Langmuir-Hinshelwood kinetic model [35]. Figure 8c shows the effect of dye concentration carried out from 2×10^{-5} to 8×10^{-5} M solution against constant catalytic load (50 mg). As the concentration of dye increases, time for the complete degradation process also increases. This is because

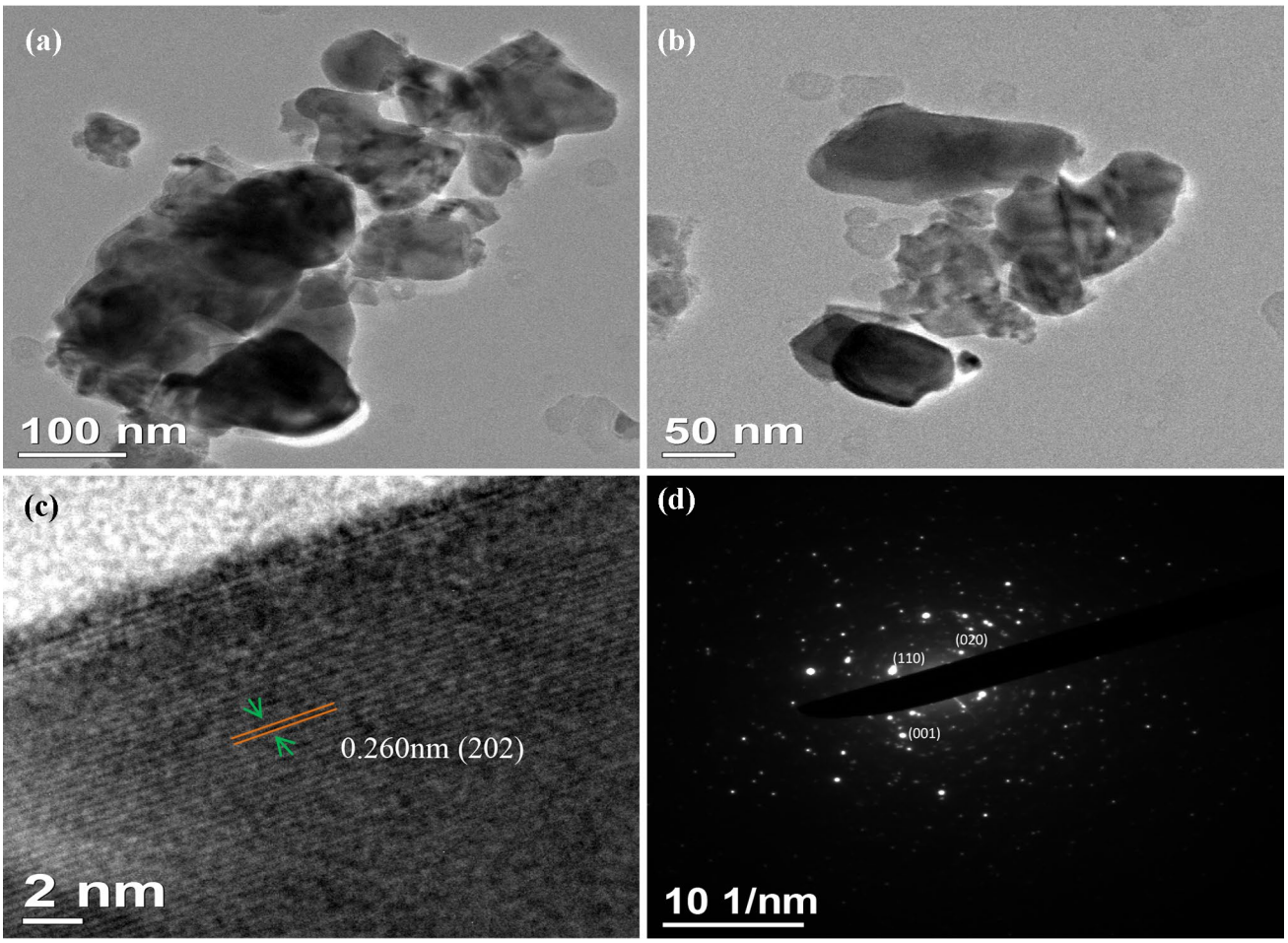

Fig. 6 **a**, **b** TEM image, **c** HRTEM and **d** SAED patterns of β-$SnWO_4$ NPs

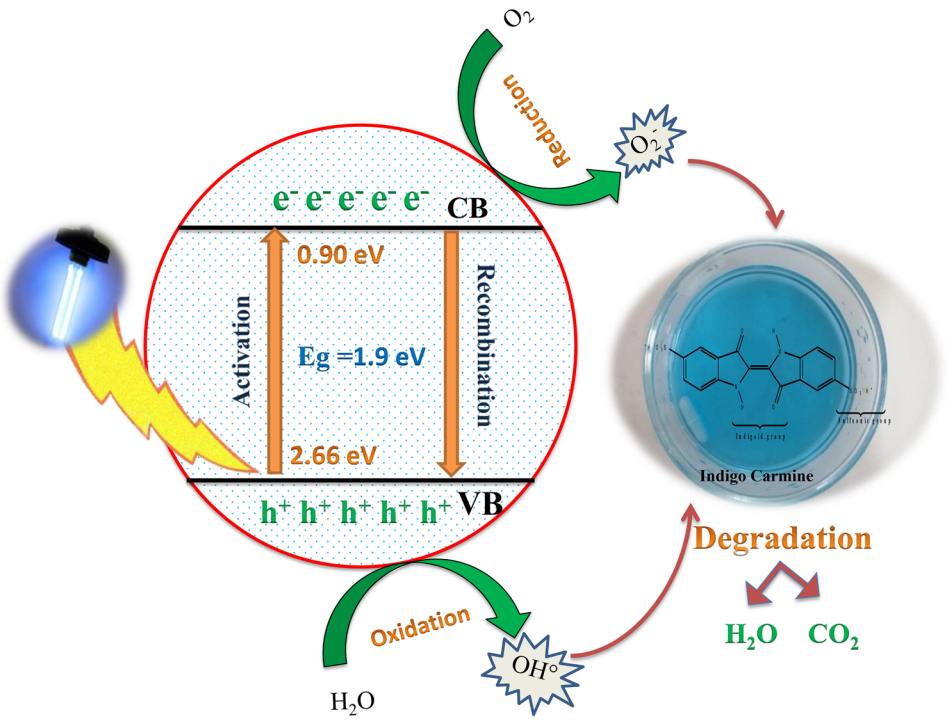

Fig. 7 Schematic representation for the IC dye degradation

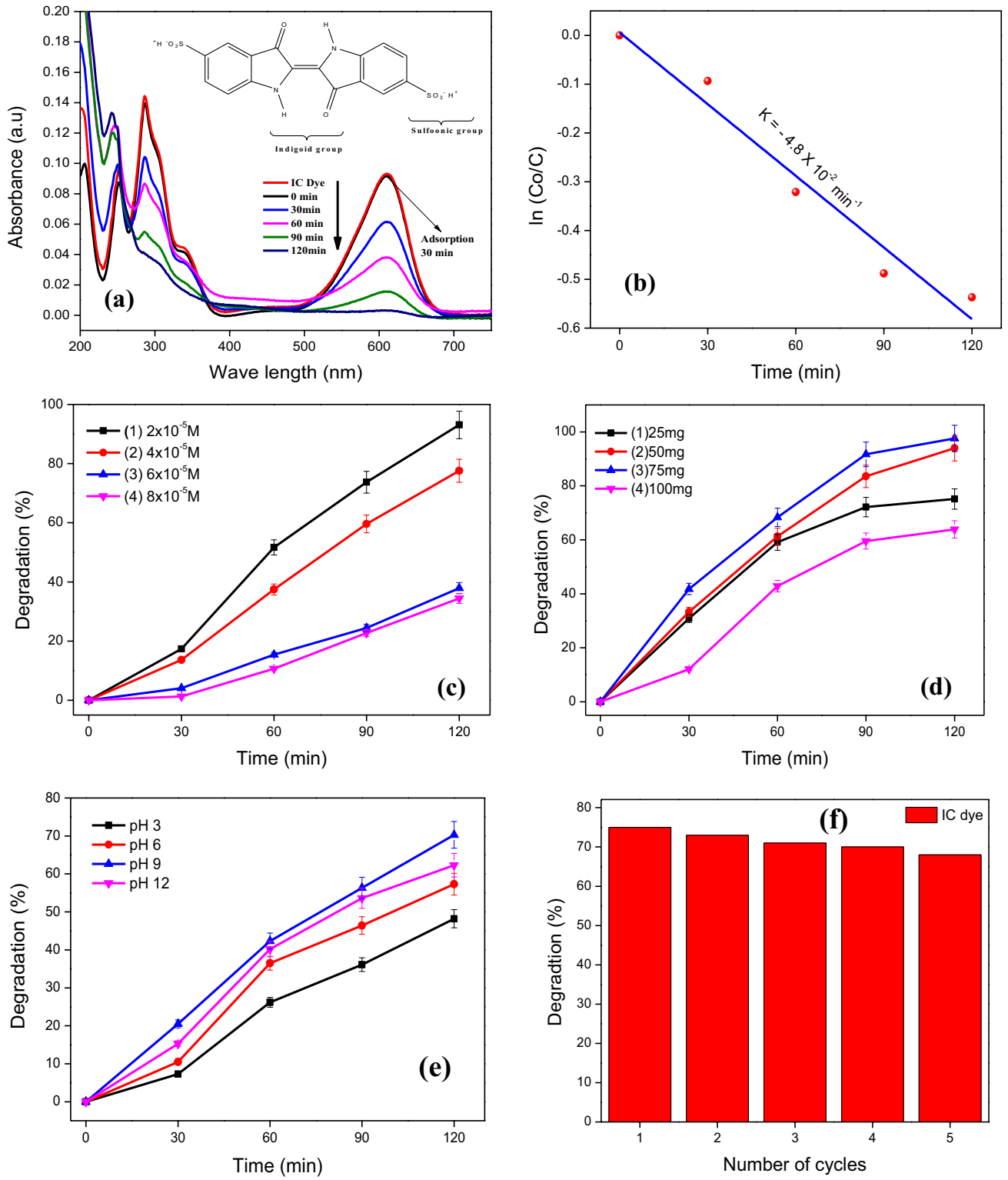

Fig. 8 **a**Time dependent photocatalytic dye degradation under Visible light irradiation **b** Kinetic study of dye degradation. **c** Photocatalytic activity of different concentrations of IC dyes at using 50 mg of β-$SnWO_4$ Nps. **d** Photocatalytic activity of 2×10^{-5} M IC dye concentration with the different catalytic load of β-$SnWO_4$ Nps. **e** Effect of pH on photocatalytic process by using β-$SnWO_4$ Nps

of fixed surface area of the catalyst. It was observed that photocatalytic efficiency was inversely proportional to its concentration of dye. As the concentration of the dye increases with constant catalyst, the number of active sites available for the dye decreases and hence the catalytic reaction will decreases. Therefore, the degradation of dye also decreases. Hence 2×10^{-5} M shows 93% of degradation and selected this dye concentration for further studies compare to higher concentration dyes.

Figure 8d shows the effect of catalytic load on the photodegradation of IC dye at 2×10^{-5} M was studied. As the catalytic load increases, photocatalytic activity also increases and reaches maximum at 75 mg of the catalyst. Further increase in catalyst, degradation efficiency decreases due to the accumulation and sedimentation of catalytic particles. Also increase in the turbidity and opacity of the suspension leads to scattering of light due to decrease in the passage of irradiation through the reaction mixture [36]. Therefore, significant photodegradation of dye was witnessed with the catalytic load of 75 mg.

Photodegradation of IC was carried out at constant dye concentration (2×10^{-5} M) and catalyst load (75 mg) by varying the pH from 3 to 12. Figure 8e clearly shows that photocatalytic process is strongly depends on the pH of the dye solution. pH of the solution was adjusted by the addition of NaOH or H_2SO_4. The variation of pH alters the surface properties of β-$SnWO_4$, in turn dissociation of the dye molecules. The highest rate of degradation was observed at pH 9. After that it starts decreasing. It can be clearly observed that degradation efficiency is more in basic than in acidic medium. Therefore increase in pH values tends to change the charge on Nps to negative by adsorbing OH^- ions, which favors the formation of OH°. The adsorbate stops the absorption of IC dye and due to electrostatic repulsion between the surface changes on the adsorbent [37]. Thus the degradation of IC dye rate was decreased above pH 9. Additionally, the increase of pH may increase e^-/h^+ recombination rate and consequently decrease the photocatalytic activity.

The photostability was evaluated by measuring the reuse of β-$SnWO_4$ Nps as shown in the Fig. 8f, after UV light irradiation for 120 min; each of the photoreaction mixture was centrifuged and filtered. β-$SnWO_4$ residue was washed several times with distilled water. Recovered β-$SnWO_4$ was then reused for new photodegradation batch, without any further treatment. All photocatalytic degradation experiments were carried out in duplicate. Many researchers examined the photostability of the catalyst and it clearly observed that the photocatalytic efficiency of β-$SnWO_4$ does not show major loss after five successive photoreaction experiments [33, 38, 39]. After the photocatalytic reactions, these β-$SnWO_4$ powders were checked again by XRD. No changes in their crystal structures were detected, tindicating the stability of these powders against visible light irradiation. Thus it is a potential photocatalyst for industrial water treatment.

The electrochemical performance of the synthesized β-$SnWO_4$ Nps has been studied with the help of cyclic voltammetric technique by considering dopamine as an analyte. The electrochemical experiments were carried out in a three electrode cell system, which contained a bare carbon paste electrode (BCPE), β-$SnWO_4$ Nps (MCPE) as the working electrode. The electrocatalytic behavior of bare and MCPE measuring 5×10^{-5} M dopamine and its CV were recorded in the range between − 0.2 to 0.6 V versus current (mA) using 0.2 M phosphate buffer solution of pH 7.2 [40]. The peak potentials for MCPE nanoparticle [ΔEp = 0.126 V] are as shown in Fig. 9a. The oxidation peak potential (Epa) of DA at BCPE and MCPE were observed at 0.1066 V and 0.1101 V respectively. Peak currents significantly increased at the MCPE with the Epa and peak currents (Ipa) increases compared to those at BCPE. These results confirmed that the presence of Nps in carbon paste electrode matrix improved the sensitivity and Nps provides a large specific area leading to the enhancement in peak current. This result indicates MCPE of Nps exhibits the good electrocatalytic activity than the bare electrode. Figure 9b shows an increase in the redox peak current at a scan rate of 0.05–0.200 V s^{-1} MCPE indicating that direct electron transfer in the modified electrode surface of dopamine [41]. 4 mg of MCPE shows maximum response current when compared to the 2, 6 and 8 mg Nps and the results are depicted in Fig. 9c and this optimized concentration is used for further investigation. Figure 9d exhibited good linearity between the scan rate and the redox peak current for the Nps MCPE with correlation coefficients of $R^2 = 0.9997$, which reveals that the electron transfer reaction was a diffusion-controlled process.

Huang Renkun et al, studied the Tin based materials like α-$SnWO_4$/rGO Nps for Li-ion batteries [42]. This article examines the lithium ion battery performances of β-$SnWO_4$ as anode. Figure 10a shows the typical CV of the synthesized β-$SnWO_4$ Nps at a scan rate of 0.01 mV s^{-1} in the potential range between 0.01–3.0 V which gives evidence for the redox couple and structural phase during the electrochemical reaction. The cell shows an open circuit voltage of roughly 3.0 V. In the cathodic sweep, an intense peak is located at ~ 2.0 V corresponding to electrochemical process resulting bare metal, amorphous Li_2O and SEI. In the anodic sweep, broad peaks appear at 0.46, 0.65 and 2.43 V correspond to oxidation of metal to metal oxide and decomposition of Li_2O. Small shifts of peaks during subsequent cycles may be due to structural and textural modifications occurred during lithiation/delithiation [43]. Coin cells CR2032 were used to assemble the cells in Argon ambient glove box (MBraun model Unilab).

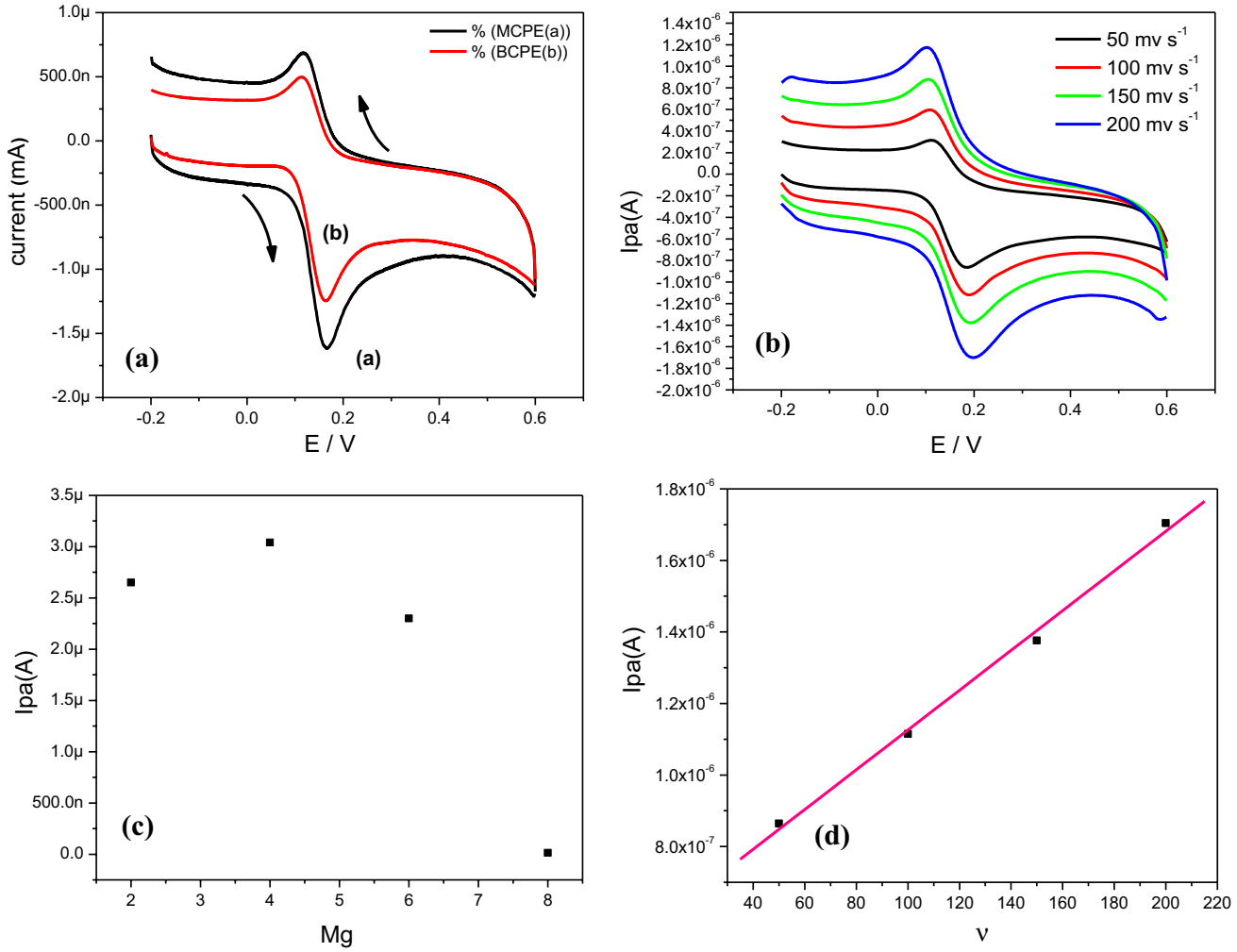

Fig. 9 **a** Cyclic Voltammogram of bare CPE and MCPE of 5×10^{-5}M DA with scan rate 50 mV s^{-1}in 0.2 M phosphate buffer solution at pH 7.2. **b** Cyclic Voltammogram of MCPE at different scan rates. **c** Response current at different concentration (2, 4, 6 and 8 mg) of β-$SnWO_4$ Nps. **d** Graph shows the linear relationship between the anodic peak current and scan

Figure 10b shows the galvanostatic charge and discharge curve of β-$SnWO_4$ Nps in the range 0.1–3.0 V at 0.1 C rate. In the first discharge, potential drops suddenly to 1.7 V and followed by the main plateau at 0.8 V showed the discharge capacity of 400 mA h g^{-1}. It is followed by another plateau at 0.2 V exhibits capacity of 800 mA h g^{-1}. Since it is oxysalt, it has shown 2 plateaus at 0.8 and 0.2 V corresponding to a reduction of tin and tungsten respectively. It showed the excess capacity of 1030 mA h g^{-1} (Theoretical capacity = 850 mA h g^{-1}). The excess capacity is may be due to the reduction of electrolyte and formation of SEI which consumes additional lithium ions. Remaining cycles follow the same path as of first representing the same process. In the first charge cycle, it showed plateaus at 0.2 V, 0.6 V and 2.0 V and delivered capacity of 603 mA h g^{-1}. This corresponds to 41% capacity loss interfacial reaction between electrode and electrolyte. The potential plateaus in galvanostatic cycling are in good agreement with cyclic voltamogram results. With cycling, reversible capacity got faded witnessing capacity of 174 mA h g^{-1} has been observed even after 100 cycles at 0.1 C current rate by retaining columbic efficiency closer to 100%. Figure 10c shows the capacity as the cycle number increases.

4 Conclusion

We have reported the synthesis of β-$SnWO_4$ Nps using cetrimide as surfactant via co-precipitation method. As-prepared sample is amorphous and calcined to 800 °C for 2 h to get crystallinity. The calcined sample ie, β-$SnWO_4$ Nps was used to examine the photocatlytic activity, electorchemical sensor and as a electrode material for

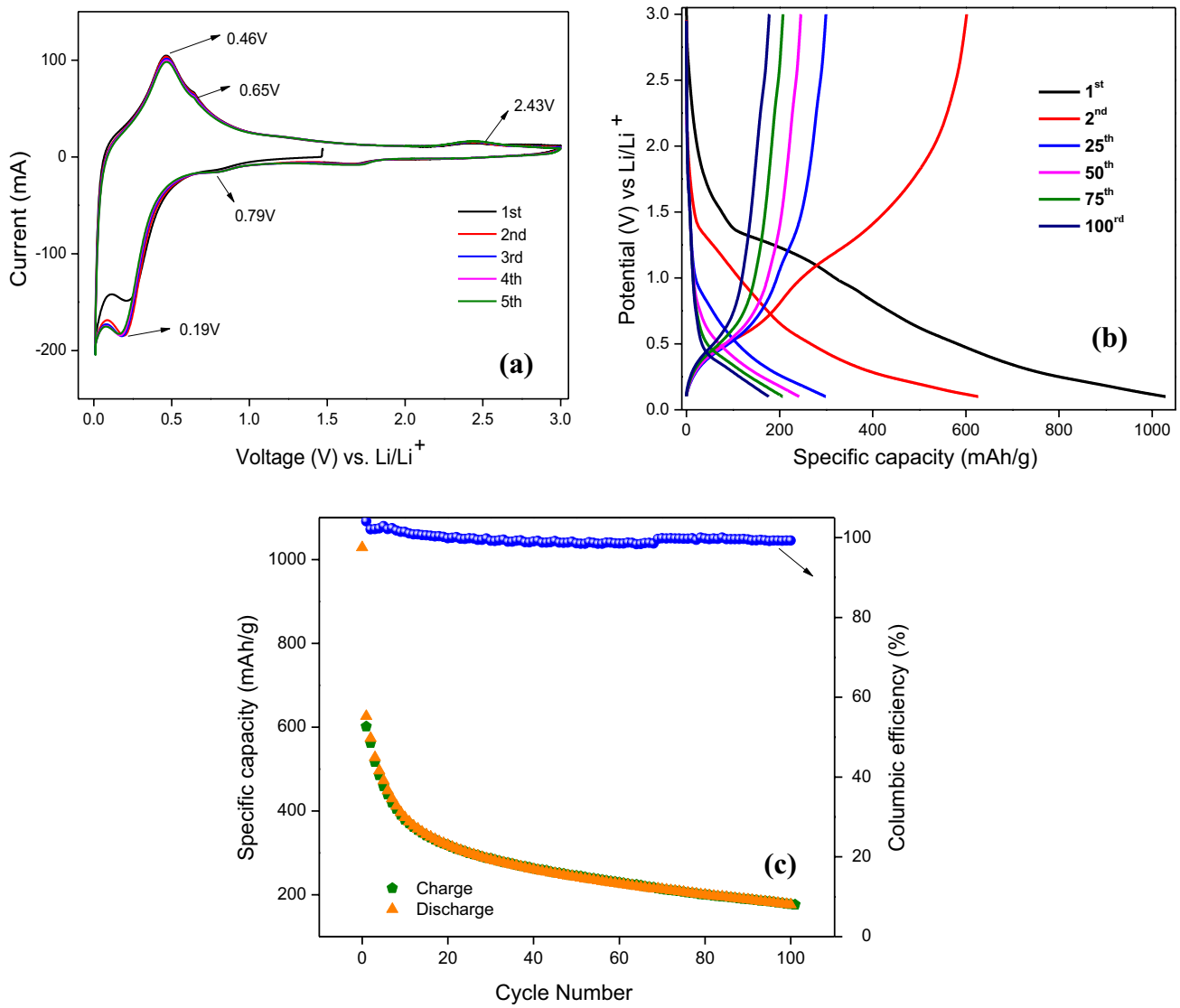

Fig. 10 **a** Cyclic Voltammogram curves of β-$SnWO_4$ Nps electrode at 0.01–3.0 V versus Li/Li^+ Scan rate 0.1 C. **b** Galvanostatic charge-discharge curves of β-$SnWO_4$ Nps at 1st, 2nd, 25th, 50th, 75th and 100 cycles between 3.0 and 0.01 V versus Li /Li^+. **c** Cycling performance and columbic efficiency at a current rate 0.1 C

lithium ion battery. 98% photocatalytic degradation of IC dye was observed for 2 h. Electrochemical behaviour of $SnWO_4$ modified carbon paste electrode shows good response towards dopamine sensing even at low concentration. LIB performance of $SnWO_4$ Nps as anode shows a reversible discharge capacity of 174 mA h g^{-1} even after 100 cycles at low scan rate indicates that it is one of the promising anode material for LIB applications.

Acknowledgements Nagaraju and Fahad A. Alharthi thanks the financial support from Kingdom of Saudi Arabia, Ministry of Education, Najran Univeristy, Promising Center for Sensors and Electronic Devices (PCSED) sanctioned on 2019 (Ref. No.: PCSED-021-18).

Compliance with ethical standards

Conflict of interest The authors declare that they have no conflict of interest.

References

1. Lv H, Liu Y, Hu J, Li Z, Lu Y (2014) Ionic liquid-assisted hydrothermal synthesis of Bi_2WO_6: reduced graphene oxide composites with enhanced photocatalytic activity. RSC Adv 4:63238–63245
2. Majhi D, Samal PK, Das K, Gouda SK, Bhoi YP, Mishra BG (2018) α-NiS/Bi_2O_3 nanocomposites for enhanced photocatalytic degradation of tramadol. ACS Appl Nano Mater 2:395–407
3. Majhi D, Bhoi YP, Samal PK, Mishra BG (2018) Morphology controlled synthesis and photocatalytic study of novel

CuS-$Bi_2O_2CO_3$ heterojunction system for chlorpyrifos degradation under visible light illumination. Appl Surf Sci 455:891–902
4. Bhoi YP, Nayak AK, Gouda SK, Mishra BG (2018) Photocatalytic mineralization of carbendazim pesticide by a visible light active novel type-II Bi_2S_3/$BiFeO_3$ heterojunction photocatalyst. Catal Commun 114:114–119
5. Das K, Majhi D, Bhoi YP, Mishra BG (2019) Combustion synthesis, characterization and photocatalytic application of CuS/$Bi_4Ti_3O_{12}$ pn heterojunction materials towards efficient degradation of 2-methyl-4-chlorophenoxyacetic acid herbicide under visible light. Chem Eng J 362:588–599
6. Bhoi YP, Behera C, Majhi D, Equeenuddin SM, Mishra BG (2018) Visible light-assisted photocatalytic mineralization of diuron pesticide using novel type II CuS/$Bi_2W_2O_9$ heterojunctions with a hierarchical microspherical structure. New J Chem 42:281–292
7. Pavithra NS, Lingaraju K, Raghu GK, Nagaraju G (2017) Citrus maxima (Pomelo) juice mediated eco-friendly synthesis of ZnO nanoparticles: applications to photocatalytic, electrochemical sensor and antibacterial activities. Spectrochim Acta Part A Mol Biomol Spectrosc 185:11–19
8. Nagaveni K, Sivalingam G, Hegde MS, Madras G (2004) Photocatalytic degradation of organic compounds over combustion-synthesized nano-TiO_2. Environ Sci Technol 38:1600–1604
9. Ajmal A, Majeed I, Malik RN, Idriss H, Nadeem MA (2014) Principles and mechanisms of photocatalytic dye degradation on TiO_2 based photocatalysts: a comparative overview. RSC Adv 4:37003–37026
10. Çeken B, Kandaz M, Koca A (2012) Electrochemical metal-ion sensor based on a cobalt phthalocyanine complex captured in Nafion® on a glassy carbon electrode. J Coord Chem 65:3383–3394
11. Hayat A, Catanante G, Marty J (2014) Current trends in nanomaterial-based amperometric biosensors. Sensors 14:23439–23461
12. Muralikrishna S, Kishore B, Nagabhushana H, Suresh D, Sharma SC, Nagaraju G (2017) One pot green synthesis of $MnCO_3$–rGO composite hybrid superstructure: application to lithium ion battery and biosensor. New J Chem 41:12854–12865
13. Tian H, Xin F, Wang X, He W, Han W (2015) High capacity group-IV elements (Si, Ge, Sn) based anodes for lithium-ion batteries. J Materiomics 1:153–169
14. Hong YJ, Son MY, Kang YC (2013) Batteries: one-pot facile synthesis of double-shelled SnO_2 yolk-shell-structured powders by continuous process as anode materials for Li-ion batteries. Adv Mater 25:2250
15. Ghannoum A, Iyer K, Nieva P, Khajepour A (2016) Fiber optic monitoring of lithium-ion batteries: a novel tool to understand the lithiation of batteries. In: IEEE sensors, pp 1–3
16. Ede SR, Kundu S (2015) Microwave synthesis of $SnWO_4$ nanoassemblies on DNA scaffold: a novel material for high performance supercapacitor and as catalyst for butanol oxidation. ACS Sustain Chem Eng 3:2321–2336
17. Li Z, Zhang Y, Xiang H, Ma X, Yuan Q, Wang Q, Chen C (2013) Trimethyl phosphite as an electrolyte additive for high-voltage lithium-ion batteries using lithium-rich layered oxide cathode. J Power Sources 240:471–475
18. Chen Y-C, Lin Y-G, Hsu L-C, Tarasov A, Chen P-T, Hayashi M, Ungelenk J, Hsu Y-K, Feldmann C (2016) β-$SnWO_4$ photocatalyst with controlled morphological transition of cubes to spikecubes. ACS Catalysis 6:2357–2367
19. Ungelenk J, Feldmann C (2012) Synthesis of faceted β-$SnWO_4$ microcrystals with enhanced visible-light photocatalytic properties. Chem Commun 48:7838–7840
20. Chandran HT, Thangavel S, Jipsa C, Venugopal G (2014) Study on inorganic oxidants assisted sonocatalytic degradation of Resazurin dye in presence of β-$SnWO_4$ nanoparticles. Mater Sci Semicond Process 27:212–219
21. Raj AT, Thangavel S, Rose A, Jipsa C, Jose M, Nallamuthu G, Kim S-J (2016) Venugopal, Influence of Morphology and Common Oxidants on the Photocatalytic Property of β-$SnWO_4$ Nanoparticles. J Nanosci Nanotechnol 16:2541–2547
22. Huang L, Yao B, Sun J, Gao X, Wu J, Wan J, Li T, Hu Z, Zhou J (2017) Highly conductive and flexible molybdenum oxide nanopaper for high volumetric supercapacitor electrode. J Mater Chem A 5:2897–2903
23. Dan M, Cheng M, Gao H, Zheng H, Feng C (2014) Synthesis and electrochemical properties of $SnWO_4$. J Nanosci Nanotechnol 14:2395–2399
24. Bakshi MS (2015) How surfactants control crystal growth of nanomaterials. Cryst Growth Des 16:1104–1133
25. Kuzmin A, Anspoks A, Kalinko A, Timoshenko J, Kalendarev R, Nataf L, Baudelet F, Irifune T, Roy P (2016) Pressure-induced insulator-to-metal transition in α-$SnWO_4$. J Phys Conf Ser 712:12122–12125
26. Goriparti S, Miele E, De Angelis F, Di Fabrizio E, Zaccaria RP, Capiglia C (2014) Review on recent progress of nanostructured anode materials for Li-ion batteries. J Power Sources 257:421–443
27. Smeets A, Evrard C, Landtmeters M, Marchand C, Knoops B, Declercq JP (2005) Crystal structures of oxidized and reduced forms of human mitochondrial thioredoxin 2. Protein Sci 14:2610–2621
28. Stoltzfus MW, Woodward PM, Seshadri R, Klepeis JH, Bursten B (2007) Structure and bonding in $SnWO_4$, $PbWO_4$, and $BiVO_4$: lone pairs vs inert pairs. Inorg Chem 46:3839–3850
29. Wojcik J, Calvayrac F, Goutenoire F, Mhadhbi N, Corbel G, Lacorre P, Bulou A (2013) Lattice dynamics of β-$SnWO_4$: experimental and Ab Initio Calculations. J Phys Chem C 117:5301–5313
30. Garadkar KM, Ghule LA, Sapnar KB, Dhole SD (2013) A facile synthesis of $ZnWO_4$ nanoparticles by microwave assisted technique and its application in photocatalysis. Mater Res Bull 48:1105–1109
31. Patil SB, Ravishankar TN, Lingaraju K, Raghu GK, Nagaraju G (2018) Multiple applications of combustion derived nickel oxide nanoparticles. J Mater Sci Mater Electron 29:277–287
32. Patil SB, Kishore B, Manjunath K, Reddy V, Nagaraju G (2018) One step hydrothermal synthesis of novel Cu_2S-MoO_3 nanocomposite for lithium ion battery and photocatalytic applications. Int J Hydrogen Energy 43:4003–4014
33. Zhu G, Que W, Zhang J, Zhong P (2011) Photocatalytic activity of $SnWO_4$ and SnW_3O_9 nanostructures prepared by a surfactant-assisted hydrothermal process. Mater Sci Eng, B 176:1448–1455
34. Gadhi TA, Hernández-Gordillo A, Bizarro M, Jagdale P, Tagliaferro A, Rodil SE (2016) Efficient α/β-Bi_2O_3 composite for the sequential photodegradation of two-dyes mixture. Ceram Int 42:13065–13073
35. Gao B, Fan H, Zhang X, Song L (2012) Template-free hydrothermal synthesis and high photocatalytic activity of $ZnWO_4$ nanorods. Mater Sci Eng B 177:1126–1132
36. Liu X, Liang B, Zhang M, Long Y, Li W (2017) Enhanced photocatalytic properties of α-$SnWO_4$ nanosheets modified by Ag nanoparticles. J Colloid Interface Sci 490:46–52
37. Yadav LR, Manjunath K, Archana B, Madhu C, Naika HR, Nagabhushana H, Kavitha C, Nagaraju G (2016) Fruit juice extract mediated synthesis of CeO_2 nanoparticles for antibacterial and photocatalytic activities. Eur Phys J Plus 131:154
38. Zhu Z, Tian H, Zhang M, Liang B, Li W (2016) Preparation of α-$SnWO_4$ hierarchical spheres by Bi3+-doping and their enhanced photocatalytic activity under visible light. Ceram Int 42:14743–14748

39. Wang QL, Li HB, Jiang HY, Ding ST, Song ZW, Shi JS (2015) Effect of solvent on α-$SnWO_4$ photocatalyst for degradation of methyl orange under visible light irradiation. Mater Technol 30:288–293
40. Kumar SK, Mamatha GP, Muralidhara HB, Anantha MS, Yallappa S, Hungund BS, Kumar KY (2017) Highly efficient multipurpose graphene oxide embedded with copper oxide nanohybrid for electrochemical sensors and biomedical applications. J Sci Adv Mater Dev 2:493–500
41. Manjunatha AS, Pavithra NS, Marappa S, Prashanth SA, Nagaraju G (2018) Green synthesis of flower-like $BiVO_4$ nanoparticles by solution combustion method using lemon (Citrus Limon) juice as a fuel: photocatalytic and electrochemical study. ChemistrySelect 3:13456–13463
42. Huang R, Ge H, Lin X, Guo Y, Yuan R, Fu X, Li Z (2013) Facile one-pot preparation of α-SnWO 4/reduced graphene oxide (RGO) nanocomposite with improved visible light photocatalytic activity and anode performance for Li-ion batteries. RSC Advances 3:1235–1242
43. Pavithra NS, Nagaraju G, Viswanatha R (2018) Surfactant assisted sonochemical synthesis of zinc tungstate nanoparticles: anode for Li-ion battery and photocatalytic activities. The European Physical Journal Plus 133:498